On-Demand Doping of Graphene by Stamping with a Chemically Functionalized Rubber Lens

Yongsuk Choi,[†,⊥] Qijun Sun,[†,⊥] Euyheon Hwang,[†,‡] Youngbin Lee,[†] Seungwoo Lee,[†] and Jeong Ho Cho*[,†,§]

[†]SKKU Advanced Institute of Nanotechnology (SAINT), [‡]Department of Physics, and [§]School of Chemical Engineering, Sungkyunkwan University, Suwon 440-746, Republic of Korea. [⊥]Y.C. and Q.S. contributed equally to this work.

ABSTRACT A customized graphene doping method was developed involving stamping using a chemically functionalized rubber lens as a novel design strategy for fabricating advanced two-dimensional (2D) materials-based electronic devices. Our stamping strategy enables deterministic control over the doping level and the spatial pattern of the doping on graphene. The dopants introduced onto graphene were locally and continuously controlled by directly stamping dopants using a chemically functionalized hemispherical rubber lens onto the graphene. The rubber lens was functionalized using two different dopants: poly(ethylene imine) to achieve n-type doping and bis(trifluoromethanesulfonyl)amine to achieve p-type doping. The graphene doping was systematically controlled by varying both the contact area (between the rubber lens and the graphene) and the contact time. Graphene doping using a stamp with a chemically functionalized rubber lens was confirmed by both Raman spectroscopy and charge transport measurements. We theoretically modeled the conductance properties of the spatially doped graphene using the effective medium theory and found excellent agreement with the experimental results. Finally, complementary inverters were successfully demonstrated by connecting n-type and p-type graphene transistors fabricated using the stamping doping method. We believe that this versatile doping method for controlling charge transport in graphene will further promote graphene electronic device applications. The doping method introduced in this paper may also be applied to other emergent 2D materials to tightly modulate the electrical properties in advanced electronic devices.

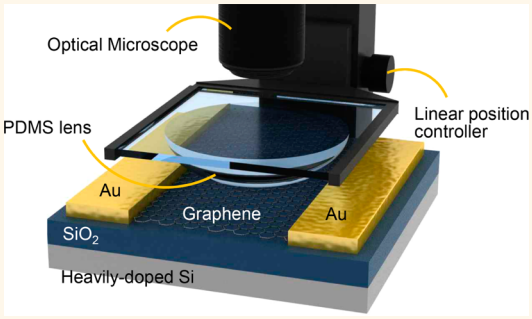

KEYWORDS: graphene · contact doping · rubber lens · dopant · complementary inverter

Graphene, a two-dimensional sp^2-hybridized single layer of carbon atoms, is a promising candidate material for use in next-generation electronics that could take advantage of its unique properties, such as its ambipolar electric field effects,[1] high carrier mobility (200 000 $cm^2 \cdot V^{-1} \cdot s^{-1}$),[2,3] anomalous quantum Hall effects,[4,5] and massless relativistic carriers.[6] Ever since graphene was first micromechanically cleaved from graphite in 2004,[1] tremendous research efforts have focused on a variety of topics in graphene chemistry, from theoretical studies[4−6] to functional device applications.[7−10] Graphene doping studies[11−16] have been critical for accurately tuning the properties of graphene, including the charge carrier density, electronic energy level, surface energy, and surface activity, all of which are fundamental to a diversity of device applications, such as transistors for logic circuits,[9,17] solar cells,[18] capacitors,[19] and sensors.[20]

Internal chemical doping/modification methods, including covalent functionalization,[21] substitutional heteroatom doping,[22] and charge transfer doping,[23,24] have been effectively utilized to tailor the electrical properties of graphene, such as the majority carrier type and concentration. However, defect formation in graphitic lattice structures accompanied by covalent functionalization and heteroatom doping suggests that charge transfer doping offers a promising approach to graphene doping. Previous studies have described successful graphene doping using a variety of dopants, such as gas molecules, organic/organometallic molecules, polymers, metals, or metal oxides.[16] These approaches present opportunities for advancing doping techniques; nevertheless,

* Address correspondence to jhcho94@skku.edu.

Received for review February 4, 2015 and accepted March 27, 2015.

Published online March 27, 2015
10.1021/acsnano.5b01791

the lack of programmable control over the site-specific doping level remains an obstacle to the manufacture of sophisticated graphene electronic device applications.

Custom doping (modulation of the doping level and position) is necessary for deterministically modulating the free carrier concentration and expanding the accessible range of electronic and optical properties. Exquisite control over the doping level and spatial position could enable the unprecedented engineering of sophisticated, translation-ready electronic devices. In this work, we first demonstrated a locally and continuously tunable graphene doping method using stamping with a chemically functionalized polydimethylsiloxane (PDMS) rubber lens. Two types of dopants were functionalized onto the rubber lenses to accomplish n-type and p-type graphene doping. The graphene doping was systematically tuned by changing both the contact area between the rubber lens and the graphene channel and the contact time. Chemical doping by the dopant-modified rubber lens was confirmed using both Raman spectroscopy and charge transport measurements. Finally, complementary inverters were successfully demonstrated by connecting n-type and p-type graphene transistors fabricated using the contact doping method. The simple and effective graphene doping method proposed in this paper will inspire new approaches to graphene doping for use in electronics applications, such as designated spot doping or high-performance graphene logic circuits.

RESULTS AND DISCUSSION

Figure 1a shows a schematic illustration of the experimental setups used to implement graphene contact doping using the chemically functionalized rubber lens. A linear translational controller with a transparent glass frame was mounted on the probe station. A glass slide with a hemispherical PDMS rubber lens was fixed onto the frame and disposed on top of the graphene channel of the graphene field-effect transistor (GFET). The rubber lens with a hemispherical shape was prepared by casting a single drop of the PDMS prepolymer onto the glass slide treated with hydrophobic trichloro(1*H*,1*H*,2*H*,2*H*-perfluorooctyl)silane (Supporting Information Figure S1). The vertical position of the PDMS lens was precisely controlled using a translational stage so that the contact area between the PDMS lens and the graphene channel was finely tuned according to the position of the glass frame. Separately, the GFETs were fabricated on the

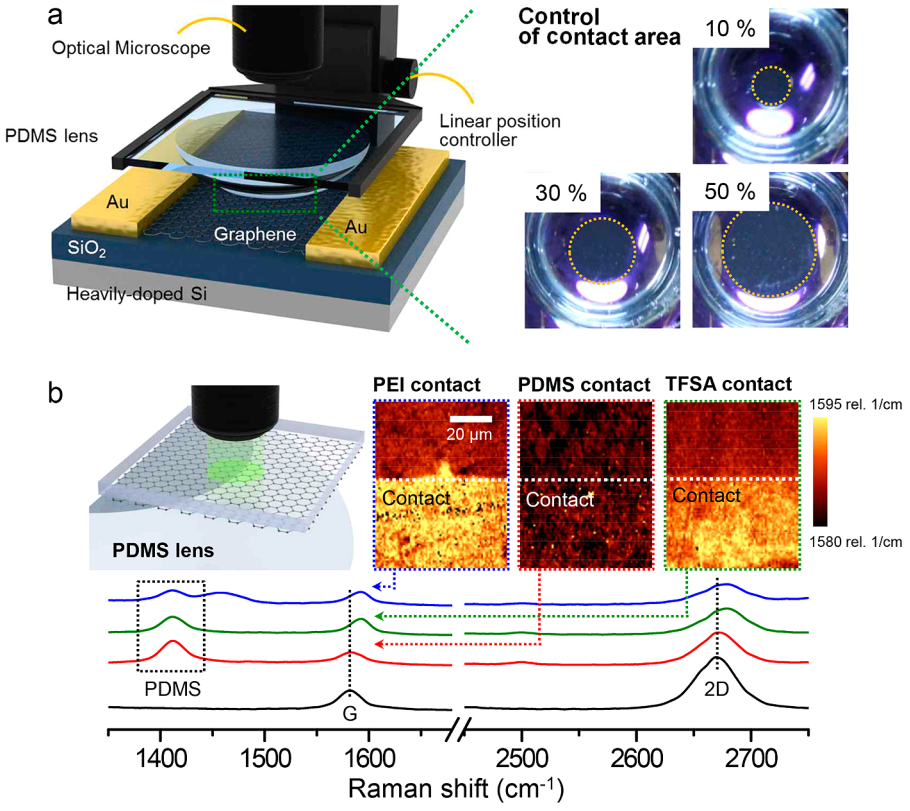

Figure 1. (a) Schematic illustration of the experimental setup of the contact doping setup using a chemically modified PDMS lens. The right panel of figure shows optical images of the contact region between the PDMS lens and the graphene channel (contact area = 10, 30, and 50%). (b) Raman spectra of the pristine graphene (black), graphene contacted with the unmodified PDMS lens (red), with the TFSA-modified PDMS lens (green), and with the PEI-modified PDMS lens (blue). The additional peak around 1450 cm^{-1} in the blue curve may be attributed to the Raman signals of PEI molecules spectroscopically enhanced by underlying graphene.[7,33] The schematic diagram shows the setup used for the Raman spectroscopy measurements collected at the edge of the contact position between the PDMS lens and the graphene.

octadecyltrichlorosilane (ODTS)-treated SiO_2/Si substrate. ODTS was utilized to minimize strong p-doping effects caused by the presence of hydroxyl groups on the SiO_2 surface. After depositing the Au/Cr source–drain electrodes, single-layer graphene grown by chemical vapor deposition (CVD) was transferred onto the substrate, and the channel region was defined by photolithography and oxygen plasma etching. The hemispherical PDMS lens, which had been treated with two types of dopants, was positioned above the graphene channel in the GFET. Poly(ethylene imine) (PEI), an amine-rich electron-donating macromolecule, was used as the n-type dopant,[25,26] and bis-(trifluoromethane sulfonyl)amine (TFSA), an electron-withdrawing molecule containing highly electronegative atoms, was used as the p-type dopant.[27,28] Conformal contact between the PDMS lens and the graphene channel was ensured by implementing linear displacement along the perpendicular direction, assisted by the linear position controller. Note that the PDMS lens can be reused several times by recoating the dopant solution onto the lens. The optical microscopy images of the PDMS lens under conditions that yielded different contact areas with the graphene channel (10, 30, or 50% of the entire graphene channel area) are shown in the right panel of Figure 1a.

The doping effects induced by local contact between the PDMS lens and the graphene channel were first investigated by Raman spectroscopy.[29−31] The Raman spectrum of the pristine graphene (black curve in Figure 1b) featured an undetectable D band and a symmetric Lorentzian-shaped 2D band centered at 2668 cm^{-1} with a full width at half-maximum of 42 cm^{-1}. The large intensity ratio of the 2D/G (I_{2D}/I_G) bands indicated the presence of high-quality single-layer graphene.[30] This configuration was constructed by applying the contact doping process to a GFET (Figure 1), and Raman measurements of the graphene doped using the PDMS lens were collected using an inverted transparent glass substrate supporting single-layer graphene, as shown in the left panel of Figure 1b. Initially, the Raman spectra of the graphene in contact with the unmodified PDMS lens did not lead to a shift in the G or 2D band positions (red curve in Figure 1b), indicating negligible doping effects. The band characteristic of PDMS at 1410 cm^{-1} appeared in all graphene samples that had undergone contact with the PDMS lens.[32] The Raman spectra of graphene films that had been contacted with PEI- and TFSA-modified PDMS lenses are indicated by the blue and red curves in Figure 1b, respectively. The G band position of the pristine graphene (black curve) at 1583 $\pm$ 2 cm^{-1} was blue-shifted to 1592 $\pm$ 1 cm^{-1} after PEI (blue curve) or TFSA (green curve) contact doping, whereas the 2D band at 2672 $\pm$ 1 cm^{-1} was blue-shifted to 2679 $\pm$ 1 cm^{-1}. The accuracy and reproducibility of contact doping using the dopant-modified PDMS lens was confirmed by the observation of significant shifts in the G and 2D band positions and the obvious decrease in I_{2D}/I_G, consistent with previously reported results.[33,34]

A Raman mapping was extracted from the G mode frequency at the edge of the contact interface between the PDMS lens and graphene, as shown in the right panel of Figure 1b. The white dotted line indicates the physical boundary of the PDMS/graphene contact interface. The high vibrational frequency is drawn in bright yellow, and the relatively low frequency is drawn in dark red, following the scale bar. The G band of the graphene region that had been contacted with the PEI- and TFSA-modified rubber lens was bright yellow (indicating a blue shift), positively affirming the successful graphene doping, whereas the graphene region that had not been contacted with the rubber lens displayed a dark red color G band that coincided with the band obtained from the graphene region that had been contacted with the unmodified PDMS lens. Importantly, the uniform bright color across the contact region indicated homogeneous doping *via* contact between the graphene and the PDMS lens.[35] In addition, chemical analysis of the contact-doped graphene films was performed by X-ray photoemission spectroscopy, which was compared with the graphene films doped by tyipical dip-coating (Supporting Information Figures S2 and S3).

Raman measurements confirmed the effectiveness of graphene doping. The dopant-modified PDMS lens was laminated on the graphene surface. Therefore, localized continuous graphene doping appeared to be achievable by controlling the contact area between the PDMS lens and the graphene channel. Figure 2a,b shows the transfer characteristics (conductance *vs* gate voltage) of the GFETs as a function of the contact area, which varied from 10 to 50% of the graphene channel area. The data points were measured after a 10 min contact time with the PDMS lens at each contact area. The calculated conductance (solid lines) is also plotted based on calculations from the experimental data sets. The transfer characteristics of the GFETs with locally doped regions were theoretically modeled using the effective medium theory (EMT).[36] A sample without local doping has a homogeneous density landscape (*i.e.*, a uniform carrier density throughout the sample) at a given gate voltage, and the measured sample conductance displays a typical V shape behavior, with a minimum conductance at the Dirac voltage. The conductance of a sample with a locally doped area displays more complicated features, however, due to the inhomogeneous density landscape created by the local doping. Two types of charge carriers with different densities may be present at a given gate voltage, leading to a mixed two-component system (Figure 2c). Thus, the overall density (or gate voltage)-dependent transport properties are complicated due

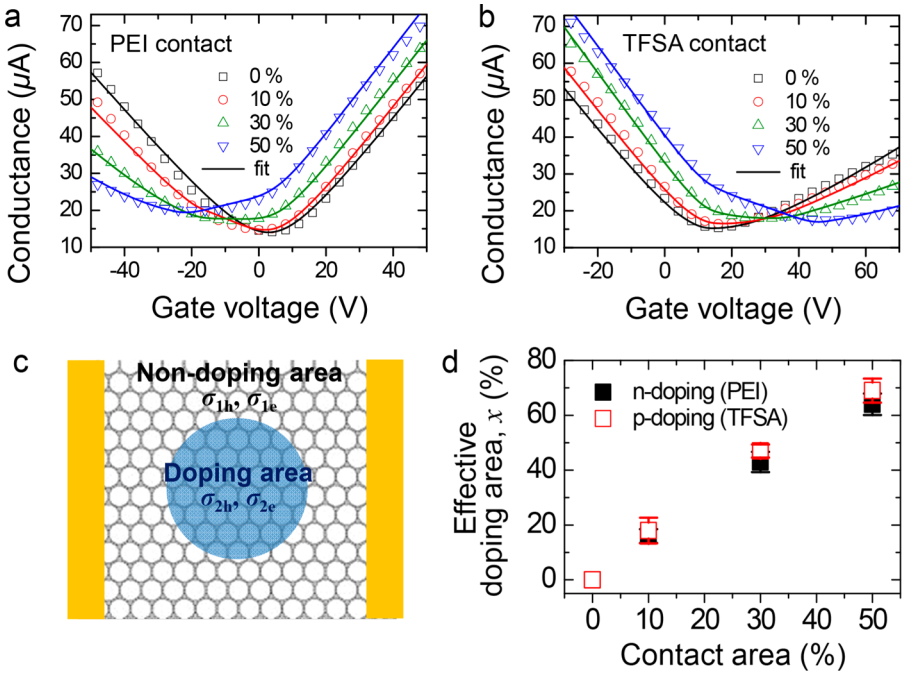

Figure 2. Electrical characteristics of the GFETs doped using the chemically modified PDMS lens. The transfer characteristics of the GFETs as a function of the contact area using (a) PEI- and (b) TFSA-modified PDMS lenses. (c) Schematic diagram of the mixed two-component system created by the local doping of the PDMS lens. (d) Effective doping area *vs* contact area between the lens and the graphene channel.

to the complex interplay between the two different carriers. The transport properties of the complex two-component system were investigated in the presence of local dopants by calculating the conductivity using the EMT, which is an excellent theory for studying the effective conductivity of nonhomogeneous media.[36−38] Our physically motivated two-component transport theory based on the coexistence of two phases of carriers in a disordered system provided a quantitative description of the experimentally observed features. For a nonhomogeneous medium with two different kinds of carriers, the effective conductivity (σ_m) is given by

$$\frac{\sigma_m - \sigma_1}{\sigma_m + \sigma_1}(1-x) + \frac{\sigma_m - \sigma_2}{\sigma_m + \sigma_2}x = 0$$

where x is the effective doping area (as discussed below) and σ_1 (or σ_2) is the conductivity of the undoped (or doped) area. The conductivity of the homogeneous region may be calculated from the Boltzmann transport theory[39] and is given by $\sigma_i = n_i e \mu_i$, where n_i and σ_i, respectively, are the carrier density and mobility of the sample (i = 1 and 2 represent the undoped and doped areas, respectively). Thus, the effective conductivity σ_m of a nonhomogeneous graphene surface may be calculated by solving the above equation self-consistently.

The solid lines in Figure 2a,b plot the calculated conductance (*i.e.*, σ_m) as a function of the gate voltage for different doping contact areas. Note that, as the contact area was varied, the mobilities in both the undoped area (μ_1) and the doped area (μ_2) remained constant because the density of charge impurities in each region remained constant and charge impurity scattering dominated the mobility measurements.[38] Thus, x was calculated by fitting the experimental data. It can be easily seen that for $x = 0$ (*i.e.*, in an undoped sample) we simply have $\sigma_m = \sigma_1$, corresponding to the conductance minimum and the Dirac voltage in the undoped area at V_{G1}. As the fraction of the locally doped area (x) increased, the conductivity curves increasingly displayed the presence of an additional feature close to the Dirac voltage of the doping area (V_{G2}), where $V_{G2} < V_{G1}$ for an n-doped sample (the PEI contact in Figure 2a) and $V_{G2} > V_{G1}$ for a p-doped sample (the TFSA contact in Figure 2b). This new feature was attributed to the minimum conductivity (maximum resistivity) at the Dirac voltage (V_{G2}) in the locally doped area. Because the dopant density in the locally doped area was irrelevant to x (the fraction of the doped area), the conductivity minimum at V_{G2} was independent of x within the experimental accuracy. Thus, the new feature appeared at V_{G2}, regardless of the value of x. Here, the values of V_G are directly related to the carrier density in the graphene channel. For PEI-contacted samples (Figure 2a), we have V_{G1} = 4 V and $V_{G2} = -20$ V, which corresponded to a hole carrier density of 2.8×10^{11} cm^{-2} and an electron carrier density of 1.4×10^{12} cm^{-2}, respectively. Thus, at a zero gate voltage, two different carriers (holes in the undoped area and electrons in the doped area) coexisted in the sample. As x increased, the measured conductance was affected more significantly by the doping contact area. As the doped area was larger than the

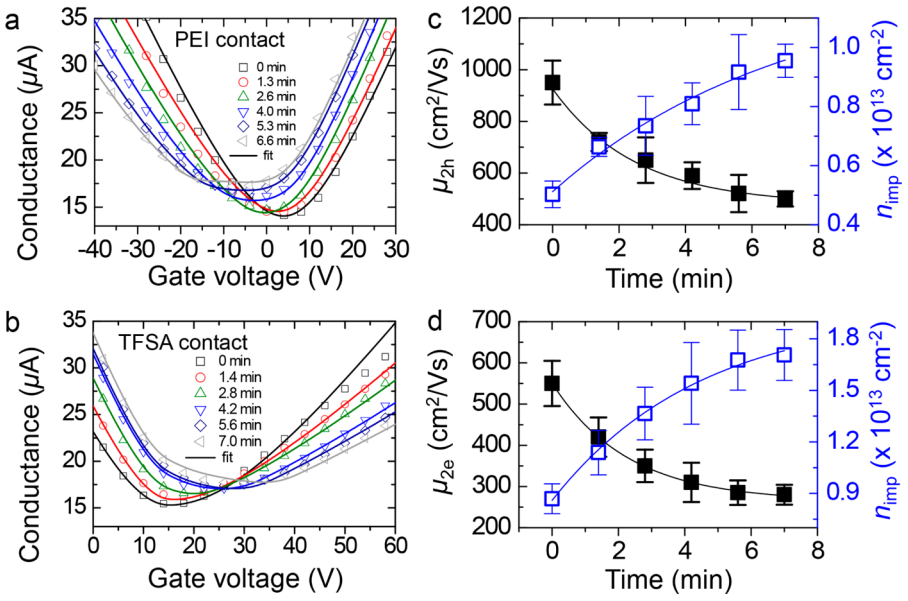

Figure 3. Transfer characteristics of the GFETs as a function of the contact time, between 0 and 6.6 min, using (a) PEI- and (b) TFSA-modified PDMS lenses (contact area = 30%). (c) Hole mobilities (μ_{2h}) and impurity densities (n_{imp}) in the area doped using the PEI-modified lens. (d) Electron mobilities (μ_{2e}) and impurity densities (n_{imp}) in the area doped using the TFSA-modified lens.

undoped area, the minimum of the total conductance shifted toward the conductance minimum, which corresponded to the Dirac point of the doped region. Thus, the conductance minimum moved to the Dirac voltage (V_{G2}) of the doping area from V_{G1}. Figure 2d plots the relationship between the effective doping area (x) and the actual contact area occupied by the PDMS lens. The variable x represents the effective fraction of the doped region that yielded σ_m, which was calculated by fitting the experimental data using the EMT model. As shown in Figure 2d, this effective doping fraction was larger than the actual contact area.

The introduction of a carrier density into graphene by the impurities was explored by measuring the time evolution of the transfer characteristics given different doping times until the characteristics had reached saturation. Figure 3a,b shows the time evolution of the conductance as a function of the gate voltage for a PEI contact (n-doping) or a TFSA contact (p-doping), respectively. The time evolution of the transfer curves was measured for a constant PDMS lens contact area of 30% ($x = 0.45$). Contact between the PDMS rubber lens introduced carriers from the PEI (or TFSA) impurities. The impurity concentration increased over time. We estimated the induced carrier density from the dopant impurities by monitoring the Dirac point shift in the transfer curve. For PEI contact (Figure 3a), the Dirac point was shifted toward negative gate voltages over time, indicating electron doping. For TFSA contact (Figure 3b), the Dirac point shifted toward positive gate voltages, indicating hole doping. In addition to the Dirac point shift, we observed a decrease in the hole (electron) mobility over time for PEI (TFSA) contact, while the electron (hole) mobility remained fixed. The increase in the carrier density (or the shift in the Dirac point) was associated with an increase in ionized dopants, which directly affected the carrier mobility. The ionized impurity densities (n_{imp}) in the doping region were estimated by calculating the time evolution of the conductance as a function of the ionized impurity density using the EMT model (see the solid lines in Figure 3a,b). Figure 3c,d shows the ionized impurity densities (n_{imp}) and the calculated mobilities of the doping areas (μ_{2h} and μ_{2e}) as a function of the contact time. The electron mobilities of the area doped (μ_{2e}) using PEI contact were calculated to be a constant value of 1049 $cm^2 \cdot V^{-1} \cdot s^{-1}$. The calculated hole mobilities (μ_{2h}) were inversely proportional to the time (from 950 to 505 $cm^2 \cdot V^{-1} \cdot s^{-1}$), as shown in Figure 3c. On the other hand, for TFSA doping, μ_{2h} was maintained at 1053 $cm^2 \cdot V^{-1} \cdot s^{-1}$, and the electron mobilities decreased from 551 to 278 $cm^2 \cdot V^{-1} \cdot s^{-1}$ over time (Figure 3d). In SiO_2, the mobility and impurity concentration are related according to $\mu = 4.78 \times 10^{15}/n_{imp}$ cm^2/V.[40,41] The carrier mobility was calculated here under the assumption that scattering occurred due to ionized charged impurity centers with a density n_{imp}. We note that the asymmetry between the electron and hole mobilities arose from the amplitude of the impurity scattering. Although changing the sign of the bias voltage does not affect the concentration of the charged impurities, it does alter the average distance between carriers on the graphene layer and the impurities.[42,43] Because the scattering amplitude due to the ionized dopants depends exponentially on the distance, for example, the positively charged dopants (after donating

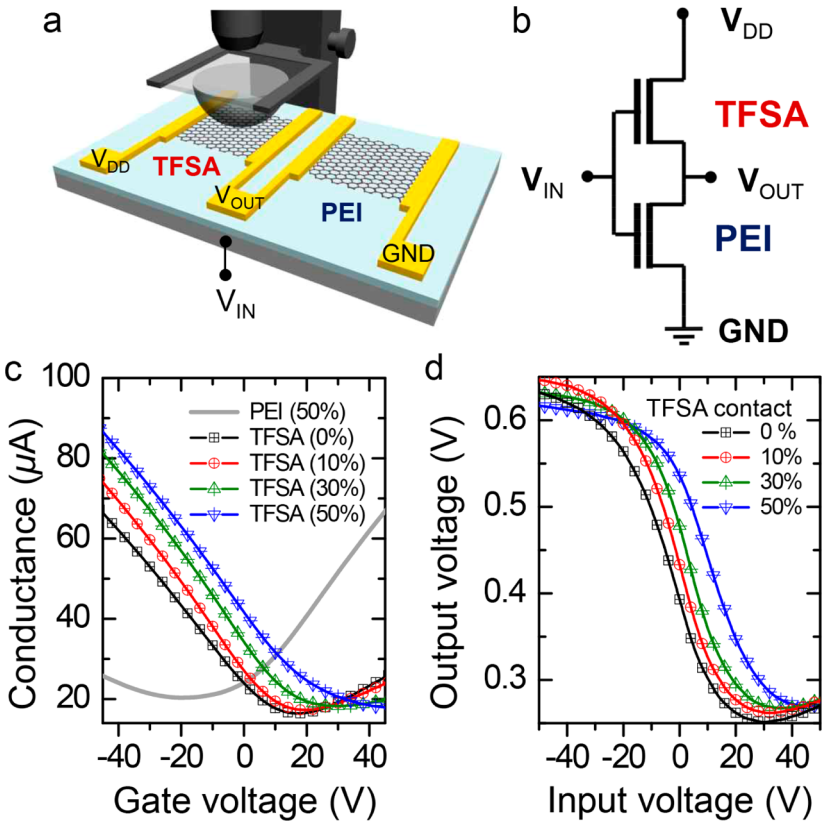

Figure 4. (a) Schematic illustration and (b) circuit diagram of the complementary inverter fabricated by contact doping. (c) Transfer characteristics of the GFETs doped with PEI (50% contact) and TFSA (0, 10, 30, and 50% contact). (d) Voltage transfer characteristics of the complementary inverters composed of n-type and n-type GFETs.

electrons) were not significantly affected by positive gate voltage; however, a negative voltage decreased the distance between the carriers and the dopants so that the scattering amplitude increased, thereby decreasing the holes mobility in the system (Figure 3c). Our observations suggested that the density of the ionized impurities after donating electrons (or holes) into the graphene sheet increased over time (t) as $n_{imp} \propto t^{1/2}$, whereas the mobility of holes (or electrons) decreased inversely with time according to $\mu \propto 1/t$ (Figure 3c,d).

Precise control over the Dirac voltage in a GFET enables the fabrication of high-performance complementary inverters composed of p-type and n-type GFETs, as is illustrated schematically in Figure 4a. Here, an n-type GFET based on a graphene channel doped with PEI (50% contact) was connected to the ground, while a p-type GFET was connected to the supply electrode. The p-type GFET was prepared using a TFSA-modified PDMS lens. The p-channel behavior of the GFET could be systematically tuned by adjusting the contact area between the lens and the GFET from 0 to 50%. The GFETs shared the same input (V_{IN}) and output terminals (V_{OUT}). The corresponding equivalent circuit diagram is shown in Figure 4b. Figure 4c shows the transfer characteristics of a single PEI-doped n-type GFET (contact = 50%) plotted as a gray solid line, and the transfer characteristics of various TFSA-doped p-type GFETs are shown as dotted lines (as the contact area was varied from 0 to 50%), measured separately. As more TFSA was applied, the curve shifted positively, indicating that the GFET doping was more p-type in character. Complementary inverters were formed based on combinations of these devices, and the corresponding voltage transfer characteristics, shown in Figure 4d, shifted in qualitative agreement with the shift plotted in Figure 4c. The agreement between the shift trends arose because signal inversion in a complementary inverter occurs at a voltage that yields the same resistance value for the n-channel and p-channel of the circuit. This voltage corresponds to the crossover point between the gray solid line and the colored dashed lines shown in Figure 4c. Although the separation between the logical levels (the difference between the ON and OFF states of the inverter) was relatively small (0.4 V in this work), the modulation of the inversion point between ON and OFF states could be precisely controlled *via* local and continuous contact doping. It is known that the charge transfer doping undergoes degradation with time, which changes the device characteristics (Supporting Information Figure S4).[44,45] Therefore, encapsulating and isolating the device are necessary to secure the device stability.

CONCLUSIONS

In summary, locally and continuously tunable doping of a GFET was demonstrated for the first time through the use of a chemically modified rubber lens (PEI to achieve n-type doping and TFSA to achieve p-type doping). Raman spectroscopy and charge transport measurements confirmed that noninvasive graphene doping using the dopant-modified PDMS lens could be used to precisely control the doping level of graphene and, thus, effectively tune charge transport in the GFETs. The effective medium theory was introduced to theoretically model the transfer characteristics of the GFET prepared with a locally doped region. Finally, a complementary inverter, which featured a precisely controlled inversion point, was successfully fabricated using the contact doping method. This work represents a significant advance in the field of graphene electronics research by offering a versatile doping method that may be useful in other materials-based devices.

EXPERIMENTAL SECTION

Graphene Growth and Device Fabrication. Large-area graphene (~10 cm^2) was grown by CVD on a Cu foil (25 μm thick) in a quartz tube. The growth temperature was maintained at 1000 °C for 30 min under a 10 sccm H_2 flow and a 5 sccm CH_4 flow. The GFETs were fabricated by first cleaning a 300 nm thick SiO_2/Si substrate with acetone, isopropyl alcohol, and deionized H_2O. An ODTS monolayer was assembled on the cleaned wafer to minimize predoping effects due to the presence of hydroxyl groups on the SiO_2 surface. Au/Cr (50 nm/5 nm) source–drain electrodes ($L/W = 1$) were thermally evaporated onto the ODTS-modified SiO_2/Si substrate in a high-vacuum environment (<10^{-6} Torr). Graphene supported by poly(methyl methacrylate) (PMMA) was then transferred onto the substrate, and the PMMA layer was subsequently removed using hot acetone (80 °C). The graphene was patterned using standard photolithography and oxygen plasma etching methods.

A 40 mM PEI (M_w = 10 000, Aldrich Inc.) ethanol solution and a 40 mM TFSA (assay 95%, Aldrich Inc.) nitromethane solution were employed as the n-type and p-type doping solutions, respectively. The hemispherical PDMS rubber lenses (diameter = 5 mm) were prepared by casting a single drop of the PDMS prepolymer (Sylgard 184, Dow Corning) onto a hydrophobic trichloro(1*H*,1*H*,2*H*,2*H*-perfluorooctyl)silane-treated glass slide and then cross-linked at 80 °C for 1 h. The PDMS rubber lens was then transferred to the glass frame of the stamping setup. Each doping solution was spin-coated onto the PDMS surface at 2000 rpm for 1 min.

Measurements. Raman spectroscopy measurements were collected using a confocal Raman microscope (Alpha 300R, Witec). Raman mapping studies were conducted using a microxy stage and a 50× objective lens with a numerical aperture of 0.55. The graphene surface (100 × 100 μm^2) in contact with the PDMS lens was scanned simultaneously with an integration time of 0.3 s and a scan rate of 3.2 μm/s. The electrical performances of the GFETs were measured at a probe station under vacuum using Keithley 2182A and Keithley 6517 units. A linear position controller mounted on the probe station was used to control the contact area between the PDMS lens and the graphene channel.

Conflict of Interest: The authors declare no competing financial interest.

Acknowledgment. This work was supported by a grant from the Center for Advanced Soft Electronics (CASE) under the Global Frontier Research Program (2013M3A6A5073177) and Basic Science Research Program (2009-0083540 and 2014R1A2A2A01006776) of the National Research Foundation of Korea (NRF) funded by the Ministry of Education, Science and Technology, Korea.

Supporting Information Available: Fabrication procedure of PDMS lens and device stability. This material is available free of charge *via* the Internet at http://pubs.acs.org.

REFERENCES AND NOTES

1. Novoselov, K. S.; Geim, A. K.; Morozov, S. V.; Jiang, D.; Zhang, Y.; Dubonos, S. V.; Grigorieva, I. V.; Firsov, A. A. Electric Field Effect in Atomically Thin Carbon Films. *Science* **2004**, *306*, 666–669.
2. Du, X.; Skachko, I.; Barker, A.; Andrei, E. Y. Approaching Ballistic Transport in Suspended Graphene. *Nat. Nanotechnol.* **2008**, *3*, 491–495.
3. Bolotin, K. I.; Sikes, K. J.; Jiang, Z.; Klima, M.; Fudenberg, G.; Hone, J.; Kim, P.; Stormer, H. L. Ultrahigh Electron Mobility in Suspended Graphene. *Solid State Commun.* **2008**, *146*, 351–355.
4. Zhang, Y. B.; Tan, Y. W.; Stormer, H. L.; Kim, P. Experimental Observation of the Quantum Hall Effect and Berry's Phase in Graphene. *Nature* **2005**, *438*, 201–204.
5. Novoselov, K. S.; McCann, E.; Morozov, S. V.; Fal'ko, V. I.; Katsnelson, M. I.; Zeitler, U.; Jiang, D.; Schedin, F.; Geim, A. K. Unconventional Quantum Hall Effect and Berry's Phase of 2π in Bilayer Graphene. *Nat. Phys.* **2006**, *2*, 177–180.
6. Novoselov, K. S.; Geim, A. K.; Morozov, S. V.; Jiang, D.; Katsnelson, M. I.; Grigorieva, I. V.; Dubonos, S. V.; Firsov, A. A. Two-Dimensional Gas of Massless Dirac Fermions in Graphene. *Nature* **2005**, *438*, 197–200.
7. Ling, X.; Xie, L. M.; Fang, Y.; Xu, H.; Zhang, H. L.; Kong, J.; Dresselhaus, M. S.; Zhang, J.; Liu, Z. F. Can Graphene Be Used as a Substrate for Raman Enhancement? *Nano Lett.* **2010**, *10*, 553–561.
8. Kim, B. J.; Jang, H.; Lee, S. K.; Hong, B. H.; Ahn, J. H.; Cho, J. H. High-Performance Flexible Graphene Field Effect Transistors with Ion Gel Gate Dielectrics. *Nano Lett.* **2010**, *10*, 3464–3466.
9. Kim, B. J.; Lee, S. K.; Kang, M. S.; Ahn, J. H.; Cho, J. H. Coplanar-Gate Transparent Graphene Transistors and Inverters on Plastic. *ACS Nano* **2012**, *6*, 8646–8651.
10. Lee, S. K.; Kim, B. J.; Jang, H.; Yoon, S. C.; Lee, C.; Hong, B. H.; Rogers, J. A.; Cho, J. H.; Ahn, J. H. Stretchable Graphene Transistors with Printed Dielectrics and Gate Electrodes. *Nano Lett.* **2011**, *11*, 4642–4646.
11. Fang, Z. Y.; Wang, Y. M.; Liu, Z.; Schlather, A.; Ajayan, P. M.; Koppens, F. H. L.; Nordlander, P.; Halas, N. J. Plasmon-Induced Doping of Graphene. *ACS Nano* **2012**, *6*, 10222–10228.
12. Peimyoo, N.; Li, J. W.; Shang, J. Z.; Shen, X. N.; Qiu, C. Y.; Xie, L. H.; Huang, W.; Yu, T. Photocontrolled Molecular Structural Transition and Doping in Graphene. *ACS Nano* **2012**, *6*, 8878–8886.
13. Yan, Z.; Sun, Z. Z.; Lu, W.; Yao, J.; Zhu, Y.; Tour, J. M. Controlled Modulation of Electronic Properties of Graphene by Self-Assembled Monolayers on SiO_2 Substrates. *ACS Nano* **2011**, *5*, 1535–1540.
14. Chua, C. K.; Pumera, M. Covalent Chemistry on Graphene. *Chem. Soc. Rev.* **2013**, *42*, 3222–3233.
15. Liu, H. T.; Liu, Y. Q.; Zhu, D. B. Chemical Doping of Graphene. *J. Mater. Chem.* **2011**, *21*, 3335–3345.
16. Maiti, U. N.; Lee, W. J.; Lee, J. M.; Oh, Y.; Kim, J. Y.; Kim, J. E.; Shim, J.; Han, T. H.; Kim, S. O. 25th Anniversary Article: Chemically Modified/Doped Carbon Nanotubes & Graphene for Optimized Nanostructures & Nanodevices. *Adv. Mater.* **2014**, *26*, 40–67.
17. Yun, J. M.; Park, S.; Hwang, Y. H.; Lee, E. S.; Maiti, U.; Moon, H.; Kim, B. H.; Bae, B. S.; Kim, Y. H.; Kim, S. O. Complementary p- and n-Type Polymer Doping for Ambient Stable Graphene Inverter. *ACS Nano* **2014**, *8*, 650–656.

18. Miao, X. C.; Tongay, S.; Petterson, M. K.; Berke, K.; Rinzler, A. G.; Appleton, B. R.; Hebard, A. F. High Efficiency Graphene Solar Cells by Chemical Doping. *Nano Lett.* **2012**, *12*, 2745–2750.
19. Wen, Z. H.; Wang, X. C.; Mao, S.; Bo, Z.; Kim, H.; Cui, S. M.; Lu, G. H.; Feng, X. L.; Chen, J. H. Crumpled Nitrogen-Doped Graphene Nanosheets with Ultrahigh Pore Volume for High-Performance Supercapacitor. *Adv. Mater.* **2012**, *24*, 5610–5616.
20. Sheng, Z. H.; Zheng, X. Q.; Xu, J. Y.; Bao, W. J.; Wang, F. B.; Xia, X. H. Electrochemical Sensor Based on Nitrogen Doped Graphene: Simultaneous Determination of Ascorbic Acid, Dopamine and Uric Acid. *Biosens. Bioelectron.* **2012**, *34*, 125–131.
21. Das, A.; Pisana, S.; Chakraborty, B.; Piscanec, S.; Saha, S. K.; Waghmare, U. V.; Novoselov, K. S.; Krishnamurthy, H. R.; Geim, A. K.; Ferrari, A. C.; et al. Monitoring Dopants by Raman Scattering in an Electrochemically Top-Gated Graphene Transistor. *Nat. Nanotechnol.* **2008**, *3*, 210–215.
22. Jin, Z.; Yao, J.; Kittrell, C.; Tour, J. M. Large-Scale Growth and Characterizations of Nitrogen-Doped Monolayer Graphene Sheets. *ACS Nano* **2011**, *5*, 4112–4117.
23. Giovannetti, G.; Khomyakov, P. A.; Brocks, G.; Karpan, V. M.; van den Brink, J.; Kelly, P. J. Doping Graphene with Metal Contacts. *Phys. Rev. Lett.* **2008**, 101.
24. Wu, Y. P.; Jiang, W.; Ren, Y. J.; Cai, W. W.; Lee, W. H.; Li, H. F.; Piner, R. D.; Pope, C. W.; Hao, Y. F.; Ji, H. X.; et al. Tuning the Doping Type and Level of Graphene with Different Gold Configurations. *Small* **2012**, *8*, 3129–3136.
25. Farmer, D. B.; Golizadeh-Mojarad, R.; Perebeinos, V.; Lin, Y. M.; Tulevski, G. S.; Tsang, J. C.; Avouris, P. Chemical Doping and Electron–Hole Conduction Asymmetry in Graphene Devices. *Nano Lett.* **2009**, *9*, 388–392.
26. Farmer, D. B.; Lin, Y. M.; Afzali-Ardakani, A.; Avouris, P. Behavior of a Chemically Doped Graphene Junction. *Appl. Phys. Lett.* **2009**, 94.
27. Kim, S. M.; Jo, Y. W.; Kim, K. K.; Duong, D. L.; Shin, H. J.; Han, J. H.; Choi, J. Y.; Kong, J.; Lee, Y. H. Transparent Organic P-Dopant in Carbon Nanotubes: Bis-(trifluoromethanesulfonyl)imide. *ACS Nano* **2010**, *4*, 6998–7004.
28. Duong, D. L.; Lee, S. M.; Chae, S. H.; Ta, Q. H.; Lee, S. Y.; Han, G. H.; Bae, J. J.; Lee, Y. H. Band-Gap Engineering in Chemically Conjugated Bilayer Graphene: *Ab Initio* Calculations. *Phys. Rev. B* **2012**, 85.
29. Ferrari, A. C. Raman Spectroscopy of Graphene and Graphite: Disorder, Electron–Phonon Coupling, Doping and Nonadiabatic Effects. *Solid State Commun.* **2007**, *143*, 47–57.
30. Ferrari, A. C.; Basko, D. M. Raman Spectroscopy as a Versatile Tool for Studying the Properties of Graphene. *Nat. Nanotechnol.* **2013**, *8*, 235–246.
31. Ferrari, A. C.; Meyer, J. C.; Scardaci, V.; Casiraghi, C.; Lazzeri, M.; Mauri, F.; Piscanec, S.; Jiang, D.; Novoselov, K. S.; Roth, S.; et al. Raman Spectrum of Graphene and Graphene Layers. *Phys. Rev. Lett.* **2006**, 97.
32. Wang, Y. Y.; Ni, Z. H.; Yu, T.; Shen, Z. X.; Wang, H. M.; Wu, Y. H.; Chen, W.; Wee, A. T. S. Raman Studies of Monolayer Graphene: The Substrate Effect. *J. Phys. Chem. C* **2008**, *112*, 10637–10640.
33. Movva, H. C. P.; Ramon, M. E.; Corbet, C. M.; Sonde, S.; Chowdhury, S. F.; Carpenter, G.; Tutuc, E.; Banerjeel, S. K. Self-Aligned Graphene Field-Effect Transistors with Polyethyleneimine Doped Source/Drain Access Regions. *Appl. Phys. Lett.* **2012**, 101.
34. Dong, X. C.; Fu, D. L.; Fang, W. J.; Shi, Y. M.; Chen, P.; Li, L. J. Doping Single-Layer Graphene with Aromatic Molecules. *Small* **2009**, *5*, 1422–1426.
35. Ni, Z. H.; Wang, Y. Y.; Yu, T.; Shen, Z. X. Raman Spectroscopy and Imaging of Graphene. *Nano Res.* **2008**, *1*, 273–291.
36. Kirkpatrick, S. Percolation and Conduction. *Rev. Mod. Phys.* **1973**, *45*, 574–588.
37. Hwang, E. H.; Das Sarma, S. Insulating Behavior in Metallic Bilayer Graphene: Interplay between Density Inhomogeneity and Temperature. *Phys. Rev. B* **2010**, 82.
38. Das Sarma, S.; Adam, S.; Hwang, E. H.; Rossi, E. Electronic Transport in Two-Dimensional Graphene. *Rev. Mod. Phys.* **2011**, *83*, 407–470.
39. Adam, S.; Hwang, E. H.; Galitski, V. M.; Das Sarma, S. A Self-Consistent Theory for Graphene Transport. *Proc. Natl. Acad. Sci. U.S.A.* **2007**, *104*, 18392–18397.
40. Xiao, S. D.; Chen, J. H.; Adam, S.; Williams, E. D.; Fuhrer, M. S. Charged Impurity Scattering in Bilayer Graphene. *Phys. Rev. B* **2010**, 82.
41. Fay, A.; Danneau, R.; Viljas, J. K.; Wu, F.; Tomi, M. Y.; Wengler, J.; Wiesner, M.; Hakonen, P. J. Shot Noise and Conductivity at High Bias in Bilayer Graphene: Signatures of Electron–Optical Phonon Coupling. *Phys. Rev. B* **2011**, 84.
42. Anicic, R.; Miskovic, Z. L. Effects of the Structure of Charged Impurities and Dielectric Environment on Conductivity of Graphene. *Phys. Rev. B* **2013**, 88.
43. Adam, S.; Hwang, E. H.; Rossi, E.; Das Sarma, S. Theory of Charged Impurity Scattering in Two-Dimensional Graphene. *Solid State Commun.* **2009**, *149*, 1072–1079.
44. Kim, K. K.; Reina, A.; Shi, Y. M.; Park, H.; Li, L. J.; Lee, Y. H.; Kong, J. Enhancing the Conductivity of Transparent Graphene Films *via* Doping. *Nanotechnology* **2010**, 21.
45. Schedin, F.; Geim, A. K.; Morozov, S. V.; Hill, E. W.; Blake, P.; Katsnelson, M. I.; Novoselov, K. S. Detection of Individual Gas Molecules Adsorbed on Graphene. *Nat. Mater.* **2007**, *6*, 652–655.